Nanoscale

ARTICLE

Wearable solid-state capacitors based on two-dimensional material all-textile heterostructures

Received 00th January 20xx,
Accepted 00th January 20xx

DOI: 10.1039/x0xx00000x

www.rsc.org/

Siyu Qiang,[a, b] Tian Carey,[b] Adrees Arbab,[b] Weihua Song,[b] Chaoxia Wang[a] and Felice Torrisi[b*]

Two dimensional (2D) materials are a rapidly growing area of interest for wearable electronics, due to their flexible and unique electrical properties. All-textile based wearable electronic components are key to enable future wearable electronics. Single component electrical elemements have been demonstrated however heterostructure-based assemblies, combining eletrically condutive and dieletric textiles such as all-textile capacitors are currently missing. Here we demonstrate a superhydrophobic conducting fabric with a sheet resistance ~2.16 kΩ $\square^{-1}$, and a pinhole-free dielectric fabric with a relative permittivity ε_r ~ 2.35 enabled by graphene and hexagonal boron nitride inks, respectively. The different fabrics are then integrated to engineer the first example of an all-textile-based capacitive heterostructure with an effective capacitance ~ 26 pF cm^{-2} and flexibility down to at least 1 cm bending radius. The capacitor sustains 20 cylces of repeated washing and more than 100 cycles of repeated bending. Finally, an AC low-pass filter with cutoff frequency ~ 15 kHz is integrated by combining the conductive polyester and the capacitor.These results pave the way toward all-textile vertically integrated electronic devices.

1 Introduction

Wearable electronics require flexibility, durability, resistance to washing, comfortable sensation and lightweight components.[1-3] In recent years, electronic textiles, or fiber-based clothing systems have emerged as the ideal platforms for future wearable electronics[4, 5] because of their softness, breathability and biocompatibility, compared to other substrates, such as plastic, paper or elastomers[6]. Electronic fabrics composing these devices encompass conductors,[7] resistors,[8] capacitors,[9] transistors,[10] have been demonstrated using metals,[11] polymers[12] or carbon-based materials[13] through various methods of textile integration, such as coating,[14] deposition,[15] spinning,[16] printing,[17] and chemical functionalization.[18] However, the stability of conductive polymer to washing strongly affects the fabric performance. For instance, ref[19] showed the resistances of conductive interconnections on textiles prepared by Poly(3,4-ethylenedioxythiophene)-poly(styrenesulfonate) (PEDOT:PSS) increased by one order of magnitude after 15 washing cycles. On the other hand, the low biocompatibility of metallic fibre composites makes them hardly compatible with biological cells. In fact, metal nanoparticles used to fabricate textile electronics such as nickel,[20] silver[21] and copper[22] all have shown cytotoxicity. Ref[22] proved that the survival of hepatocytes (i.e. liver cells) after exposure to Cu nanoparticles was no more than 60% as assessed by MTT (3-(4,5-dimethylthiazol-2-yl)-2,5-diphenyltetrazolium bromide) assay (which is a method to assess cell metabolic activity).[23] In addition, the hydrophobic property of fabrics are highly common on technical textiles and would have significant role on protecting wearable electronics[24] and improve their washability, thus making it a requirement.

Graphene and other two-dimensional (2D) materials show outstanding thermal, electrical, optical and mechanical properties,[25] and they can be easily processed in solution[26] in large quantities[27,28] to produce printable inks[29,30] and thin films.[31] The environmental-stability and biocompatibility of graphene inks[32,33] has recently sparked huge interest in the textile industry enabling environmentally-friendly, bendable, and washable conductive fabric[34] and polymer.[35] Examples of graphene-based conductive textiles[36,37] currently employ graphene oxide (GO) because of its oxygen functional groups such as epoxide (C-O-C), hydroxyl (-OH), and carboxyl (-COOH),[36] providing strong affinity to cotton, wool and silk textiles, via hydrogen bonding. The GO fabric usually requires a chemical or thermal reduction step, to improve the conductivity, during the graphene fabric manufacturing process,[38,39] however high temperature and strong chemical reactions might damage the textile fibers.[40,41] Recently, a graphene-cotton strain sensor with sheet resistance (R_s) as low as 500 Ω $\square^{-1}$ has been demonstrated using a low-temperature (180 °C) reduced graphene oxide (RGO) coating via hot-press [34]. However, RGO still retained a more defective structure than the pristine graphene counterpart. In this regard, fabric

[a] Key Laboratory of Eco-Textile, Ministry of Education, School of Textiles and Clothing, Jiangnan University, 1800 Lihu Road, Wuxi 214122, China. Email: wangchaoxia@sohu.com
[b] Cambridge Graphene Centre, Department of Engineering, University of Cambridge, 9 JJ Thomson Avenue, Cambridge CB3 0FA, UK. Email: ft242@cam.ac.uk

incorporating pristine graphene could offer a cheap and environment-friendly option for highly conducting and flexible textiles, while avoiding the reduction step.

The future development of wearable electronic textiles requires also indispensable components such as charge storage devices in the form of textiles, able to store electric,[42,43] thermal,[44] solar energy.[45] CNT/graphene hybrid textile electrodes and a filter paper separator are reported to operate as flexible and wearable electrochemical capacitors in Na_2SO_4 electrolyte.[46] However, capacitors using aqueous electrolytes have handling difficulties and the potential risk of leakage,[47] making it incompatible with wearable devices. Pristine graphene and hexagonal boron nitride (h-BN) inks produced by liquid-phase exfoliation (LPE) have enabled printed graphene/h-BN/graphene solid state capacitor on PET,[48] and graphene/h-BN heterostructure FETs and integrated circuits on textile,[30]. Despite these advances, the combination of electrical textile components into an electronic textile heterostructure is still missing from literature and will be essential to advance the functionality of wearable electronics.

Here we demonstrate conducting graphene/polyester and dielectric h-BN/polyester textiles by uniformly coat polyester fabric with graphene and h-BN inks. The two functional textiles are then vertically stacked into an all-fabric graphene/h-BN capacitor heterostructure achieving a capacitance of ~ 26 pF cm^{-2}.

2 Results and discussion

2.1 Graphene and h-BN Inks

We prepare the graphene and h-BN inks by ultrasonication of graphene nanoplatelets (GNP) in ethanol and h-BN flakes in deionized water respectively (see 'Methods'). We disperse the flakes in solvents with a low boiling point (< 101 °C) to easily enable solvent removal at room temperature, hastening the throughput of the 'dip and dry' process. The concentrations of GNP (c_{GNP}) and h-BN ($c_{h\text{-}BN}$) flakes in the inks are estimated from the optical absorption spectra of GNP (black curve) and h-BN (red curve) inks in Fig. 1(a) via the Beer-Lambert law. Considering the absorption coefficients (at 660 nm) of GNP (2460 L g^{-1} m^{-1})[26] and h-BN (2350 L g^{-1} m^{-1}) [49] with the respective dilution ratio, we obtain cGNP ~ 3.77 mg ml^{-1} and ch-BN ~ 0.20 mg ml^{-1}.

We monitor the quality of GNP and h-BN flakes by Raman spectroscopy. Fig. 1(b) shows characteristic peaks of GNP at ~ 1337, ~ 1574 and ~ 2687 cm^{-1} (black curve), which correspond to the D, G, and 2D band, respectively. While G peak is always present in GNP, originating from the E_{2g} phonon vibration mode, the D peak is activated by a defect.[50, 51] However we mainly attribute the origin of most of these defects to the edges of GNP, rather than to defects in the basal plane.[52] The 2D peak is the second order resonance of the G peak and no defects are required for its activation. For the h-BN (red curve), a single peak appears at ~ 1367 cm^{-1} corresponding to E_{2g} phonon vibration mode.[53,54]

The atomic force microscopy (AFM) statistics reveal the lateral size (S) and thickness (t) of GNP and h-BN flakes. Figure 1c shows the distributions of the lateral size of GNP (black) and h-BN flakes (red), respectively. The log-normal fits (black and red curves) are peaked at ~ 2189 nm and ~ 567 nm, respectively. Figure 1d plots the thickness distributions of GNP (black) and h-BN (red) flakes, respectively. The log-normal fit is peaked at ~ 5 nm for GNP (black curve), ~ 31 nm for h-BN flakes (red curve), indicating the presence of single and multi-layer flakes with an average number of layers per flake of ~ 12 for GNP, and ~ 89 for h-BN, assuming an approximate 1 nm water layer[55] and interlayer distance of 0.34 nm.

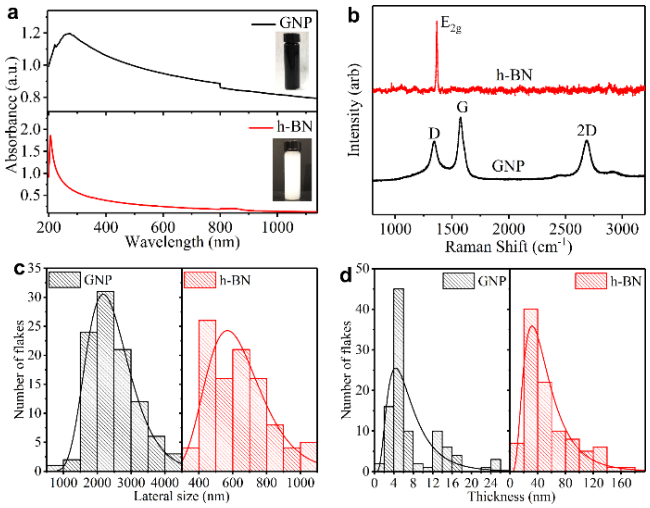

Fig. 1 (a) The optical absorption spectra of ethanol-based GNP ink (black curve) and water-based h-BN ink (red curve). (b) The Raman spectra of GNP (black curve) and h-BN (red curve) flakes acquired on Si/SiO_2 substrate. The (c) lateral size and (d) thickness log-normal distributions of GNP and h-BN flakes from atomic force microscopy statistics.

2.2 GNP/polyester and h-BN/polyester Fabrics

'Dip and dry' process is a one-step common approach to deposit functional materials on textile by immersion into solution followed by solvent removal. We prepare GNP/polyester and h-BN/polyester fabrics as follows. We use repeated 'dip and dry' processes (see 'Methods') of a pristine polyester fabric in GNP and h-BN inks respectively, obtaining GNP textile (GNP/polyester) from GNP ink and polyester, and h-BN textile (h-BN/polyester) from h-BN ink and polyester. An additional hot-press (200 °C) step on GNP/polyester is performed to enhance the adhesion between GNP and polyester, following the strategy proposed in ref.[56]

The preparation of both functional textiles is monitored and characterized by optical microscopy, SEM, electrical and contact angle measurements as follows. Fig. 2(a) shows the optical image of the white pristine polyester fabric, which then is coated by GNP ink in Fig. 2(b). Fig. 2(c) shows the SEM micrograph of the pristine polyester fabric organized in a

compact woven textile with fiber size ranging from 15 to 20 µm, while Fig. 2(d) shows the SEM micrograph of GNP/polyester fabric coated with 10 repeated cycles of GNP by 'dip and dry' process. The fabric surface is uniformly covered with the GNP deposited layer and both the weave structure and the gaps between the fibers can hardly be seen after the coating. Similar results have been reported by ref[14] for graphene nanosheets coated onto polyester fabric by a similar 'dip and dry' method, which are attributed to the strong adhesion of graphene nanosheets on polyester via the strong Van Der Waals interactions between them, as well as between neighbouring graphene nanosheets.[57]

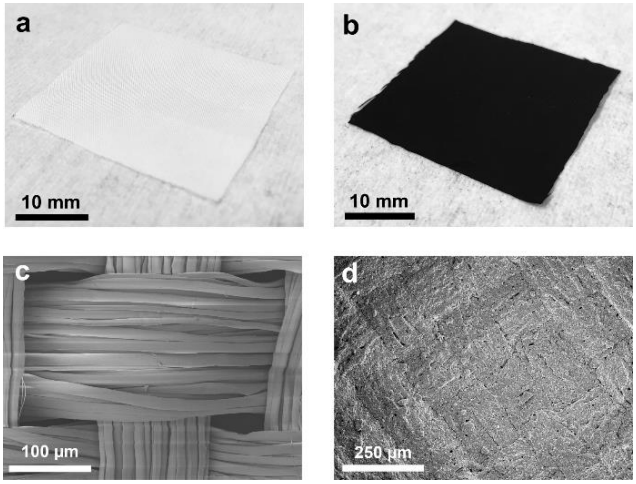

Fig. 2 The optical microscopy of (a) pristine polyester fabric and (b) polyester fabric coated by GNP ink. The SEM micrographs revealing the micromorphology of (c) pristine polyester and (d) GNP/polyester (after 10 cycles of 'dip and dry' GNP coating).

We also monitor the mass loading (m_{GNP}) of GNPs onto GNP/polyester fabric as a function of 'dip and dry' process cycles from Fig. 3(a). Importantly, we notice that the mGNP as a function of coating cycles increases almost linearly (where the red line shows the linear fit in Fig. 3(a)) over 10 cycles and eventually reaching ~ 1 mg cm^{-2}.

The electrical properties of the GNP/polyester fabric are then investigated by measuring R_s as a function of the 'dip and dry' cycles as shown in Fig. 3(b). The R_s decreases asymptotically reaching a stable value after 7 cycles, going from R_s ~ 573 MΩ □$^{-1}$ after the 1st cycle (mGNP ~ 0.11 mg cm^{-2}), to R_s ~ 15.78 kΩ □$^{-1}$ after the 8th cycle (mGNP ~ 0.80 mg cm^{-2}) and R_s ~ 15.13 kΩ □$^{-1}$ after the 10th cycle (mGNP ~ 1.06 mg cm^{-2}). We limit the coating cycle repetitions to 10 due to the negligible reduction in R_s beyond the 7th cycle (< 3.9 % from the 8th cycle to the 10th cycle).

Temperature annealing via hot-press has shown to improve the adhesion of a graphene-based ink coating onto a fabric substrate.[56] We treat our GNP/polyester with a hot-press step (4 min at 200 °C) to promote the adhesion between graphene flakes and polyester fabric. Considering the pristine polyester melting point between 205 to 260 °C, we select 200 °C as suitable hot-press temperature that approaches the melting to improve adhesion, but not beyond the melting temperature to avoid weakening the mechanical property of polyester fabric. Then we investigate the R_s of GNP/polyester (m_{GNP} ~ 1.06 mg cm^{-2}) as a function of hot-press time. Fig. 3(c) shows R_s decreasing from ~ 6.21 kΩ □$^{-1}$ (after 30 sec annealing), to ~ 4.68 kΩ □$^{-1}$ (after 2 min annealing) before plateauing to ~ 2.16 kΩ □$^{-1}$ (beyond 3 min annealing). The little increase on R_s from 3 min to 5 min of hot-press is irrelevant as their values fall within the error bars. Fig. 3(d) exhibits the comparison of the SEM cross sectional micrographs of GNP/polyester before and after the hot-press step (200 °C, 4 min), with an evident difference in the micromorphology of the fabric.

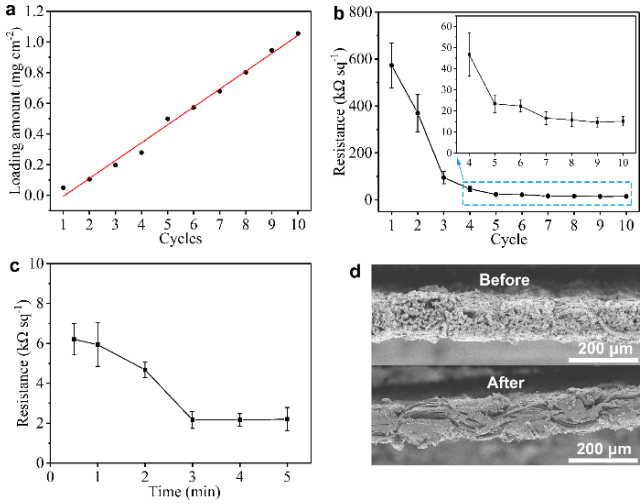

Fig. 3 (a) The GNP loading as a function of 'dip and dry' cycles, where the red line shows the linear fit. Plots of Rs of GNP/polyester as a function of (b) 'dip and dry' cycles from 1 to 10 (the insert shows a zoom in the range of 4 to 10 cycles), and (c) hot-press time across 5 min. (d) The comparison of cross-sectional SEM micrographs of GNP/polyester before and after the hot-press step (200 °C, 4 min).

Such difference in micromorphology caused by the hot-press step has already been reported for pristine graphene/cotton[56] and GO/cotton fabrics.[34] This could certainly contribute to improve the conductivity of our GNP/polyester as already demonstrated for graphene inks.[56] However, given the almost irrelevant R_s reduction in the first minute of heat-treatment, we tend to exclude a main role of the mechanical pressure as we rather attribute the R_s reduction to an improvement of the crystallinity of the GNP flakes. This is further supported by the Raman spectra (in the 1000 – 2000 cm^{-1} region, Fig. 4(a)) of GNP/polyester, as a function of hot-press time. The inset shows the reduction in the ratio of the intensity of D peak, I(D) over the intensity of the G peak, I(G) as a function of the hot-press time. I(D)/I(G) decreases from ~ 0.85 before hot-press treatment to ~ 0.5 between 1 – 5 min of hot press time, suggesting a slight increase in the average size of the sp^2 domains and deoxygenation in the functional groups,[29] as shown for a GO/cotton fabric in our previous work.[34]

Hydrophobicity is key to protect wearable electronics. Fig. 4(b) shows water droplets spherically assembled on a GNP/polyester after the hot-press step confirming water-resistant performance. To further investigate the hydrophobic properties of our fabric, we measure the contact angle (*CA*) and sliding angle (*SA*) of GNP/polyester, before and after the hot-press step. Fig. 4(c) and (d) show the *CA* (black curve) and *SA* (blue curve) as a function of 'dip and dry' cycles and hot-press time, respectively. Before the hot-press step, the GNP/polyester (m_{GNP} ~ 1.06 mg cm^{-2}) shows *CA* ~ 141.41° and SA ~ 21°, while the pristine polyester only possess *CA* ~ 80°. The hot-press step (4 min) causes it to reach *CA* ~ 153.28° and SA ~ 5°, consistent with a superhydrophobic behavior (which is defined as a surface displaying a *CA* of water greater than 150° and a *SA* less than 10°),[58] which is generally formed by a hydrophobic materials with rough micro/nanostructures.[59] It is worth noting that functional fabrics prepared by coating GO or RGO on textile achieved a maximum *CA* of ~ 143° [60] and ~ 140°,[61] respectively. Hence, the super-hydrophobic behaviour in our GNP/polyester fabric results from the lower amount of hydrophobic polar groups on hot-pressed GNPs with respect to RGO.

The h-BN/polyester was also prepared by repeated 'dip and dry' coating process of polyester fabric in h-BN ink. The h-BN mass loading ($m_{h\text{-}BN}$) reaches 0.76 mg cm^{-2} after 12 cycles, but can hardly be increased by further coating cycles. The thickness (*t*) of h-BN/polyester is *t* ~ 0.04 mm.

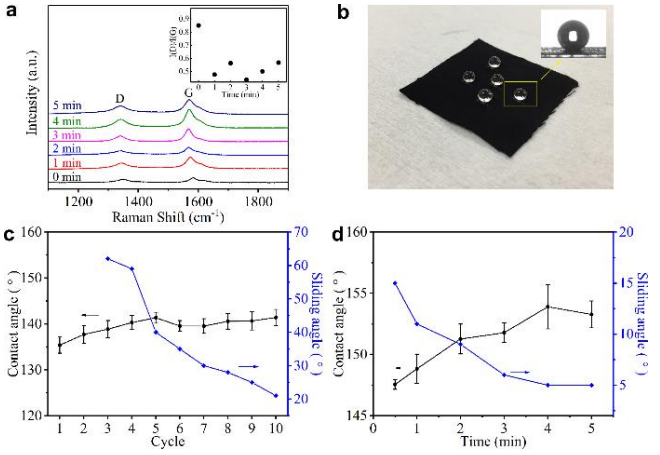

Fig. 4 (a) The Raman spectra (in the 1000 – 2000 cm^{-1} region) of GNP/polyester as a function of hot-press time. (b) The GNP/polyester (m_{GNP} ~ 1.06 mg cm^{-2}) hydrophobic property after the hot-press step (200 °C, 4 min). The *CA* (black curves) and *SA* (blue curves) as a function of (c) 'dip and dry' cycles from 1 to 10, and (d) hot-press time.

2.3 Flexible Textile-Based Capacitor

The flexible textile-based capacitor (FTC) is composed of the GNP/polyesters (*Rs* ~ 2.16 kΩ □$^{-1}$, *CA* ~ 153.28°, *SA* ~ 5°) and the h-BN/polyester ($m_{h\text{-}BN}$ ~ 0.76 mg cm^{-2}, *t* ~ 0.04 mm) as electrodes and dielectric layers, respectively. We design the FTC by stacking these functional textiles to form a conductive/dielectric/conductive (CDC) sandwich-like heterostructure, resembling that of a typical parallel plate capacitor, following the schematic in Fig. 5(a). The CDC heterostructure is sealed at the edges with 0.1 mg of polyurethane (Puruikai Co.,Ltd, China), to avoid disturbing the contact between fabrics. Then it is pressed mechanically using a Manual Hydraulic Press (Specac, UK) at 5 kPa for 1 min at ambient temperature, to improve adhesion between the layers. Subsequently, we heat the CDC heterostructure at 70 °C for 1 h to anneal the polyurethane and create the FTC. Fig. 5(b) shows the cross-section images of the FTC heterostructure. The specific design of the FTC is described in Fig. 5(c), where the h-BN/polyester dielectric has a lager width (*w* ~ 1.5 cm) than the GNP/polyester (*w* ~ 1.0 cm), resulting in an area of the capacitor (*A*) of ~ 1 cm2 (1 cm × 1 cm).

We also consider the case where the pristine polyester and CMC present in the dielectric fabric may affect the capacitance. Hence, to quantify the effect of h-BN on the dielectric layer of the textile capacitor, we create a control capacitor (FCC) using same GNP/polyester electrodes and a polyester dielectric fabric coated with CMC only in the same proportion used for the FTC, but excluding the h-BN flakes. Impedance spectroscopy (IS) is used to characterise the capacitance of FTC and FCC as it is most accurate at measuring capacitances in the pF range, typically not achievable by cyclic voltammetry (CV). [30]Bode plots of FTC and FCC are shown in Fig. 5(d) and (e), where the impedance amplitude ($|Z|$) as a function of frequency is measured with an impedance analyzer. Using an equivalent circuit model of a resistor and capacitor (*R*-*C*) in series, the impedance amplitude can be expressed as $|Z| = (R^2 + (2\pi f C)^{-2})^{0.5}$, where *Z* is the impendence, *R* is the series resistance, *f* is the frequency and *C* is the capacitance.[48] The capacitance per unit area of the FTC (CFTC) is ~ 26 pF cm^{-2} while the FCC only shows a maximum capacitance (CFCC) of ~ 5 fF cm^{-2}, demonstrating that the charge storage contribution due to the CMC polymer is negligible, and CFTC is mainly originating from the presence of h-BN flakes.

We can estimate the approximate relative permittivity (ε_r) of h-BN/polyester from the relationship formula: $\varepsilon_r = C\, d\, (\varepsilon_0\, A_{eff})^{-1}$,[48] where the *d* is distance between two electrodes, the ε_0 is the permittivity of the vacuum and A_{eff} is the effective area of the capacitor. However, the texture and roughness of the GNP/polyester and h-BN/polyester can make partial, full or no contact with each other in the FTC, thus affecting A_{eff}. This is confirmed by the roughness of the weave observed on surface of GNP/polyester (m_{GNP} ~ 0.69 mg cm^{-2}) in Fig. 5(f) and the clear textile of 'hills' and 'valleys' in the GNP/polyester and h-BN/polyester (see Fig. 5(b)) caused by the weave. To quantify this contribution on the final A_{eff}, we describe the woven structure of the textile as shown in Fig. 5(g). The whole fabric can be subdivided into many repeated units as red squares (area of single red square is marked as A_0), where four 'hills' (light red squares) exist in single repeated units and their area are marked as A_1, A_2, A_3, A_4, separately. We then define the contact ratio (*CR*) as $(A_1+A_2+A_3+A_4)/A_0$, which results in *CR* = 0 when $A_1+A_2+A_3+A_4 = 0$ (i.e. no contact between GNP/polyester and h-

BN/polyester, giving A_{eff} = 0) and CR = 1 when $A_1+A_2+A_3+A_4 = A_0$ (i.e. full contact between GNP/polyester and h-BN/polyester is made, giving $A_{eff} = A$). We estimated a CR ~ 0.5 by contrast analysis (see 'Methods') on SEM micrographs, acquired on GNP/polyester and h-BN/polyester (Fig. 1S) meaning A_{eff} = 0.5 A. Using C ~ 26 pF cm^{-2}, A ~ 0.5 cm^2, ε_0 ~ 8.854 × 10-12 F m^{-1} and d ~ 0.04 mm as the values for our FTC, we obtain approximate relative permittivity of εr ~ 2.35 for h-BN/polyester, which is in line with values reported previously for h-BN inks (*i.e.* ε_r ~ 2 – 8) [30, 48] and greater than the dielectric permittivity of polyester (ε_r ~ 1.44).[62]

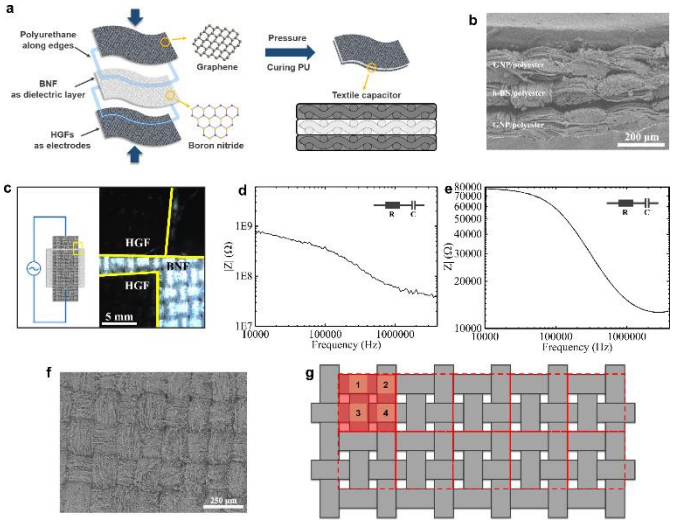

Fig. 5 (a) The schematic of the textile-based capacitor integrating GNP/polyesters as electrodes and h-BN/polyester as dielectric. (b) The cross-sectional SEM micrograph of FTC showing the functional textile heterostructure. (c) The layout of FTC (left) showing h-BN/polyester and CMC/polyester optical image (right). Typical Bode plots obtained for (d) FCC and (e) FTC, which follow an *R-C* equivalent circuit model. (f) The top-view SEM micrograph of GNP/polyester (m_{GNP} ~ 0.69 mg cm^{-2}) and (g) the diagram of the weave in the fabric with the repeating units in red.

The flexibility (measured in terms response to uniaxial bending) is an important performance metric for wearable electronics. The flexibility of the GNP/polyester electrodes and the FCT is tested by measuring R_s and C, respectively, as a function of different bending radii (using rods from 3.0 to 1.0 cm diameter). Fig. 6(a) shows a photograph of the GNP/polyester (m_{GNP} ~ 1.06 mg cm^{-2}, after 4 min of hot-press) under 180° bending. Fig. 6(b) shows the R_s change (R/R_0), defined as the value of R_s (R) upon bending over the original value of R_s (R_0) as a function of bending radius, where the ∞ corresponds to the GNP/polyester in its original flat state. We obtained R/R_0 ~ 0.93 at a bending radius of 1.0 cm, demonstrating a negligible change in R_s with bending, compared to recently reported R_s response to bending of am RGO-coated cotton fabric showing more than one order of magnitude at a bending radius of 2.5 cm.[34] This large change was attributed to the cracking and subsequent sliding and rearranging of the fractured islands of RGO film under tension.[34] Here we attribute the small R_s change to the transition between cracks and overlaps[34] on the conductive coating of textile. As described in Fig. 6(c), there is a counterbalancing effect between the two sides of the fabric upon bending. The cracks on the compressed side of GNP/polyester tend to be narrower and eventually overlap, resulting in a reduced R_s. On the other hand, the cracks on the side under tension would widen, thus resulting in an increase of R_s, which compensates the overall resistance keeping R_s unchanged.

We also tested the flexibility of FTC (C ~ 17.83 pF cm^{-2}), under the same bending condition as above. Fig. 6(d) shows an image of FTC while bending. The C change (C/C_0, defined as the value of C upon bending over the original value of C) of FTC is presented in Fig. 6(e) as a function of the bending radius. The estimated C/C_0 is less than 4% across different bending radii: ~ 0.99 (radius ~ 3.0 cm), ~ 1.02 (radius ~ 2.5 cm), ~ 0.98 (radius ~ 2.0 cm), ~ 0.97 (radius ~ 1.5 cm), ~ 1.03 (radius ~ 1.0 cm). It is important to note that C in our devices is acquired while bending, unlike previous reports where C acquisition is performed after bending.[63-65,66] The FTC in our work shows a consistent response under flexion, which is essential in textile electronics. We further investigate the stability of FTC after repeated bending and washing cycles. The FTC (see Supplementary Information) can sustain 20 cycles of repeated washing and more than 100 cycles of repeated bending.

In order to demonstrate the potential applications of FTC, we designed an all-textile AC low-pass filter device. The R-C series filter is composed of an FTC (C ~ 11.82 pF) and a GNP/polyester fabric engineered to match a resistance of 1.5 MΩ. The response versus frequency in decibel (Bode plot) of the filter (fig. 6f) shows a typical curve of a low-pass filter with a cutoff frequency at ~ 15 kHz, from the formula of $f = (2\pi RC)^{-1}$. [67]

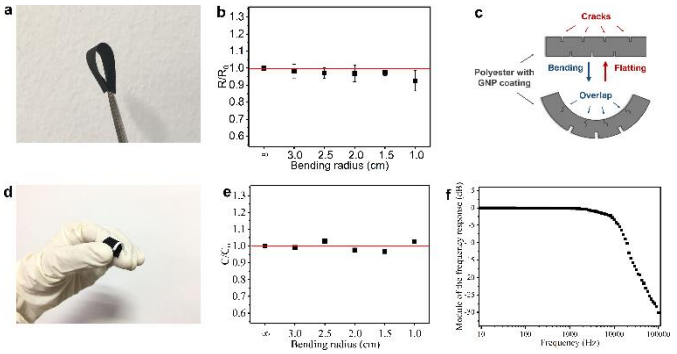

Fig. 6 (a) The GNP/polyester upon 180° bending. (b) The R/R_0 of GNP/polyester as a function of bending radius. (c) The proposed mechanism resulting in negligible R_s change in GNP/polyester during bending. (d) The FTC upon bending. (e) The C/C_0 of FTC as a function of bending radius. (f) An all-textile AC low-pass R-C filter.

3 Methods

3.1 Formulation of GNP and h-BN Inks

The graphene (Cambridge Nanosystems, GR1) produced by cracking methane and carbon dioxide in a plasma torch, are dispersed in ethanol via ultrasonic bath (Fisherbrand FB15069, 800 W) for 3 h to create a GNP ink. The h-BN flakes are dispersed in deionized water via ultrasonic bath for 24 h with carboxymethylcellulose sodium salt (CMC, average molecular weight MW = 700,000) (4 mg ml^{-1}) as polymer stabilization agent.[30] Then the h-BN dispersion is centrifuged (Beckman Coulter Proteomelab XL-A, with a SW 32 Ti swinging bucket rotor) at 3000 rpm for 20 min, and the top 80% of the centrifuged dispersion is collected for further characterization.

3.2 Preparation of Conductive and Dielectric Textiles

Commercial polyester fabrics (unit mass of 6.73 mg cm^{-2}) are cleaned by deionized water to remove the dust and contaminants, and then is dried. Subsequently, the cleaned polyester fabrics (1 cm × 2 cm), are immersed into the GNP ink with continuous stirring for 3 min, then transferred on glass slides and dried in an oven at 60 °C for 5 min to evaporate the ethanol solvent. The above process is defined as 'dip and dry' coating and can be repeated for several cycles to prepare GNP/polyester with a higher concentration of GNP flakes. The fabrication of h-BN/polyester is similar to that of GNP/polyester, using 12 cycles of repeated 'dip and dry' processes by h-BN ink (with 4 mg ml^{-1} CMC). The hot-press step of GNP/polyester is set at 200 °C on a Pixmax G3 SWING 38.

3.3 Characterization

The R_s of GNP/polyester is tested by a source measure unit SMU Instruments (KEITHLEY 2400 SourceMeter, US) and a multimeter (Resistance Model ~ 10 kΩ, 100 kΩ, Extech Instruments, US). The capacitances of the FTC and the FCC are estimated by Bode plots by using an impedance analyzer (Agilent 4294A Precision Impedance Analyzer). The *CA* and *SA* tests on GNP/polyesters are performed by a Drop Shape Analyzer 100 (KRÜSS GmbH, Germany), using deionized water droplets at ambient temperature in volume of 5 μL and 10 μL, respectively. The weight of textile is measured by using an Automatic Weighing machine (Sartorius weighing technology GmbH, Germany). The thickness of h-BN/polyester is determined using a YG141 Fabric-Thickness Gauge (Ningfang Company, China). The bending tests on GNP/polyesters and FTCs are carried by adhering them onto rods with bending radius of 1.0, 1.5, 2.0, 2.5, 3.0 cm, while the repeated bending test is carried on FTC with bending radius of 1.0 cm. The UV–vis absorption spectra of GNP and h-BN inks are measured on an Agilent Technologies Cary 7000 with wavelength from 200 nm to 1400 nm. The flake concentration of the GNP ink and h-BN ink can be estimated via the Beer-Lambert law that $A = \alpha cl$, where A is the absorbance, l is the light path length, c is the concentration of dispersed flakes, and α is the absorption coefficient.[68] The GNP and h-BN inks are diluted 1:100 and 1:20 with ethanol and water/CMC, respectively. The Raman spectra using to monitor the quality of GNP and h-BN flakes, is acquired using a Renishaw inVia Raman spectrometer (Renishaw PLC, UK) with a 514 nm laser. A Bruker Dimension Icon Atomic Force Microscope (AFM) in Peak Force Tapping mode is used to estimate the lateral size and thickness distribution of GNP and h-BN flakes, where the statistics are based on 100 individual flakes. The lateral size S of flake is defined as $S = (xy)^{0.5}$, where x and y are the length and width of flake. The average number of flake layers on ink are calculated by assuming an approximate 1 nm water layer[55] and an interlayer distance of 0.33 nm for GNP, 0.55 nm for h-BN flake). The scanning electron microscope (SEM) images of pristine polyester fabric, GNP/polyester are characterized on a sigma HD FE-SEM unit (FEI Magellan 400L XHR, US). The cross-section SEM images of GNP/polyester before and after hot-press step, and FTC are characterized on a SU1510 SEM unit (Hitachi, Ltd, Japan). The optical images of GNP/polyester and FTC are caught by an Optiphot 300 (Nikon, Japan). The SEM images of GNP/polyester (mGNP ~ 0.69 mg cm^{-2}) are used to estimate the A_0, A_1, A_2, A_3, A_4 of each repeated unit, where the CR of capacitor is determined from average value of $(A_1+A_2+A_3+A_4)/A_0$ from 15 individual repeated units. In washing test, a waterproof polyurethane-protective layer (WBM Seam Tapes) was hot pressed (PixMax Swing heat press) around the top and bottom of the FTC at 120 °C for 5 s in-line with current industry standards to protect textile eletronics. The sample was then placed inside a rotawash washing fastness tester (Skyline, SL-F09) to wash the sample for 20 cycles according to the international standard ISO105-C06-A1S.

Conclusions

In this work, we have reported a highly flexible, conductive, superhydrophobic polyester fabric (sheet resistance of ~ 2.16 kΩ $\square^{-1}$, contact angle of ~ 153.28°, sliding angle of ~ 5°) and a flexible dielectric polyester fabric (approximate relative permittivity ~ 2.35) by simple 'dip and dry' coating of graphene ink and h-BN ink, respectively. We use these functional fabrics to assemble the first all-textile flexible capacitive heterostructure, demonstrating an effective capacitance of ~ 26 pF cm^{-2} and robust flexibility (down to bending radius of 1 cm) that the capacitor can undergo repeated washing and bending test. An application of AC low-pass filter is demonstrated by combining the conductive polyester and the capacitor heterostructure. Our results demonstrate the key role of 2D materials in the development of wearable electronics, and set the ground for new strategies for the integration of two-dimensional materials with textiles to create unique devices.

Acknowledgements

The authors acknowledge the financial support of the EPSRC (grant EP/P02534X/1), the Royal Academy of Engineering Enterprise Scheme, National Natural Science Foundation of China (21174055), the Graduate Students Innovation Project of Jiangsu Province in China (SJLX16_0483), the national first-class discipline program of Light Industry Technology and Engineering

(LITE2018-21), the Trinity College, Cambridge, the Isaac Newton Trust, and the International Joint Research Laboratory for Advanced Functional Textile Materials.

Notes and references

1. M. Amjadi, K. U. Kyung, I. Park and M. Sitti, Adv. Funct. Mater., 2016, 26, 1678-1698.
2. F. Axisa, P. M. Schmitt, C. Gehin, G. Delhomme, E. McAdams and A. Dittmar, IEEE Transactions on information technology in biomedicine, 2005, 9, 325-336.
3. G. Zhou, F. Li and H.-M. Cheng, Energy & Environmental Science, 2014, 7, 1307-1338.
4. Y. Yang, Q. Huang, L. Niu, D. Wang, C. Yan, Y. She and Z. Zheng, Adv. Mater., 2017, 29.
5. W. Zeng, L. Shu, Q. Li, S. Chen, F. Wang and X. M. Tao, Adv. Mater., 2014, 26, 5310-5336.
6. M. Gao, L. Li and Y. Song, J. Mater. Chem. C, 2017, 5, 2971-2993.
7. H. Cheng, C. Hu, Y. Zhao and L. Qu, NPG Asia Materials, 2014, 6, e113.
8. J. Lilja and P. Salonen, Electronics Letters, 2011, 47, 602-604.
9. M. Stoppa and A. Chiolerio, Sensors, 2014, 14, 11957-11992.
10. M. Maccioni, E. Orgiu, P. Cosseddu, S. Locci and A. Bonfiglio, Applied Physics Letters, 2006, 89, 143515.
11. C.-H. Xue, J. Chen, W. Yin, S.-T. Jia and J.-Z. Ma, Appl. Surf. Sci., 2012, 258, 2468-2472.
12. C. Cochrane, V. Koncar, M. Lewandowski and C. Dufour, Sensors, 2007, 7, 473-492.
13. H. Lee, H. Kim, M. S. Cho, J. Choi and Y. Lee, Electrochimica Acta, 2011, 56, 7460-7466.
14. G. Yu, L. Hu, M. Vosgueritchian, H. Wang, X. Xie, J. R. McDonough, X. Cui, Y. Cui and Z. Bao, Nano letters, 2011, 11, 2905-2911.
15. Y. Li, X. Cheng, M. Leung, J. Tsang, X. Tao and M. Yuen, Synthetic metals, 2005, 155, 89-94.
16. Z. Dong, C. Jiang, H. Cheng, Y. Zhao, G. Shi, L. Jiang and L. Qu, Adv. Mater., 2012, 24, 1856-1861.
17. Y. Mao, M. Zhu, W. Wang and D. Yu, Soft. Matt., 2018.
18. J. Cao and C. Wang, Appl. Surf. Sci., 2017, 405, 380-388.
19. M. Åkerfeldt, A. Lund and P. Walkenström, Text. Res. J., 2015, 85, 1789-1799.
20. R. Shukla, V. Bansal, M. Chaudhary, A. Basu, R. R. Bhonde and M. Sastry, Langmuir, 2005, 21, 10644-10654.
21. K. Soto, K. Garza and L. Murr, Acta Biomaterialia, 2007, 3, 351-358.
22. T. Wang, X. Chen, X. Long, Z. Liu and S. Yan, PloS one, 2016, 11, e0149484.
23. M. Ahamed, M. A. Siddiqui, M. J. Akhtar, I. Ahmad, A. B. Pant and H. A. Alhadlaq, Biochemical and biophysical research communications, 2010, 396, 578-583.
24. S. Gorgutsa, K. Bachus, S. LaRochelle, R. D. Oleschuk and Y. Messaddeq, Smart Materials and Structures, 2016, 25, 115027.
25. K. Novoselov, Reviews of Modern Physics, 2011, 83, 837.
26. Y. Hernandez, V. Nicolosi, M. Lotya, F. M. Blighe, Z. Sun, S. De, I. McGovern, B. Holland, M. Byrne and Y. K. Gun'Ko, Nature nanotechnology, 2008, 3, 563.
27. K. R. Paton, E. Varrla, C. Backes, R. J. Smith, U. Khan, A. O'Neill, C. Boland, M. Lotya, O. M. Istrate and P. King, Nature materials, 2014, 13, 624.
28. P. G. Karagiannidis, S. A. Hodge, L. Lombardi, F. Tomarchio, N. Decorde, S. Milana, I. Goykhman, Y. Su, S. V. Mesite and D. N. Johnstone, ACS nano, 2017, 11, 2742-2755.
29. F. Torrisi, T. Hasan, W. Wu, Z. Sun, A. Lombardo, T. S. Kulmala, G.-W. Hsieh, S. Jung, F. Bonaccorso and P. J. Paul, ACS nano, 2012, 6, 2992-3006.
30. T. Carey, S. Cacovich, G. Divitini, J. Ren, A. Mansouri, J. M. Kim, C. Wang, C. Ducati, R. Sordan and F. Torrisi, Nature Communications, 2017, 8, 1202.
31. D. Purdie, D. Popa, V. Wittwer, Z. Jiang, G. Bonacchini, F. Torrisi, S. Milana, E. Lidorikis and A. Ferrari, Applied Physics Letters, 2015, 106, 253101.
32. E. B. Secor, T. Z. Gao, A. E. Islam, R. Rao, S. G. Wallace, J. Zhu, K. W. Putz, B. Maruyama and M. C. Hersam, Chemistry of Materials, 2017, 29, 2332-2340.
33. D. McManus, S. Vranic, F. Withers, V. Sanchez-Romaguera, M. Macucci, H. Yang, R. Sorrentino, K. Parvez, S.-K. Son and G. Iannaccone, Nature nanotechnology, 2017, 12, 343.
34. J. Ren, C. Wang, X. Zhang, T. Carey, K. Chen, Y. Yin and F. Torrisi, Carbon, 2017, 111, 622-630.
35. F. Torrisi, D. Popa, S. Milana, Z. Jiang, T. Hasan, E. Lidorikis and A. C. Ferrari, Advanced Optical Materials, 2016, 4, 1088-1097.
36. J. W. Jeon, S. Y. Cho, Y. J. Jeong, D. S. Shin, N. R. Kim, Y. S. Yun, H. T. Kim, S. B. Choi, W. G. Hong and H. J. Kim, Adv. Mater., 2017, 29.
37. R. Jalili, S. H. Aboutalebi, D. Esrafilzadeh, R. L. Shepherd, J. Chen, S. Aminorroaya-Yamini, K. Konstantinov, A. I. Minett, J. M. Razal and G. G. Wallace, Adv. Funct. Mater., 2013, 23, 5345-5354.
38. D. R. Dreyer, S. Park, C. W. Bielawski and R. S. Ruoff, Chemical Society Reviews, 2010, 39, 228-240.
39. S. Pei and H.-M. Cheng, Carbon, 2012, 50, 3210-3228.
40. L. Cabrales and N. Abidi, Journal of thermal analysis and calorimetry, 2010, 102, 485-491.
41. H. Zhao, J. H. Kwak, Z. C. Zhang, H. M. Brown, B. W. Arey and J. E. Holladay, Carbohydrate polymers, 2007, 68, 235-241.
42. Y. Yang, Q. Huang, L. Niu, D. Wang, C. Yan, Y. She and Z. Zheng, Adv. Mater., 2017, 29, 1606679.
43. L. Bao and X. Li, Adv. Mater., 2012, 24, 3246.
44. A. Jamekhorshid, S. Sadrameli and M. Farid, Renewable and Sustainable Energy Reviews, 2014, 31, 531-542.
45. Y.-H. Lee, J.-S. Kim, J. Noh, I. Lee, H. J. Kim, S. Choi, J. Seo, S. Jeon, T.-S. Kim and J.-Y. Lee, Nano letters, 2013, 13, 5753-5761.
46. H. Cheng, Z. Dong, C. Hu, Y. Zhao, Y. Hu, L. Qu, N. Chen and L. Dai, Nanoscale, 2013, 5, 3428-3434.
47. S. Yamazaki, A. Takegawa, Y. Kaneko, J.-i. Kadokawa, M. Yamagata and M. Ishikawa, Electrochemistry Communications, 2009, 11, 68-70.
48. A. G. Kelly, D. Finn, A. Harvey, T. Hallam and J. N. Coleman, Applied Physics Letters, 2016, 109, 1400-3493.
49. J. Shen, Y. He, J. Wu, C. Gao, K. Keyshar, X. Zhang, Y. Yang, M. Ye, R. Vajtai and J. Lou, Nano letters, 2015, 15, 5449-5454.
50. A. Ferrari and J. Robertson, Physical Review B, 2001, 64, 075414.
51. A. C. Ferrari and J. Robertson, Physical review B, 2000, 61, 14095.
52. V. Bianchi, T. Carey, L. Viti, L. Li, E. H. Linfield, A. G. Davies, A. Tredicucci, D. Yoon, P. G. Karagiannidis and L. Lombardi, Nature Communications, 2017, 8, 15763.
53. R. V. Gorbachev, I. Riaz, R. R. Nair, R. Jalil, L. Britnell, B. D. Belle, E. W. Hill, K. S. Novoselov, K. Watanabe and T. Taniguchi, Small, 2011, 7, 465-468.
54. S. Reich, A. Ferrari, R. Arenal, A. Loiseau, I. Bello and J. Robertson, Physical Review B, 2005, 71, 205201.
55. A. G. Kelly, T. Hallam, C. Backes, A. Harvey, A. S. Esmaeily, I. Godwin, J. Coelho, V. Nicolosi, J. Lauth and A. Kulkarni, Science, 2017, 356, 69-73.
56. P. Cataldi, L. Ceseracciu, A. Athanassiou and I. S. Bayer, ACS Appl. Mat. Interfaces, 2017, 9, 13825-13830.
57. J. Zhao, W. Ren and H.-M. Cheng, J. Mater. Chem. A, 2012, 22, 20197-20202.
58. S. Qiang, K. Chen, Y. Yin and C. Wang, Mater. Des., 2017, 116, 395-402.
59. H. Wang, Y. Xue, J. Ding, L. Feng, X. Wang and T. Lin, Angew. Chem. Int. Ed., 2011, 50, 11433-11436.

60. N. D. Tissera, R. N. Wijesena, J. R. Perera, K. N. de Silva and G. A. Amaratunge, Appl. Surf. Sci., 2015, 324, 455-463.
61. K. Krishnamoorthy, U. Navaneethaiyer, R. Mohan, J. Lee and S.-J. Kim, Applied Nanoscience, 2012, 2, 119-126.
62. S. Sankaralingam and B. Gupta, IEEE Transactions on Instrumentation and Measurement, 2010, 59, 3122-3130.
63. G. Wang, H. Wang, X. Lu, Y. Ling, M. Yu, T. Zhai, Y. Tong and Y. Li, Adv. Mater., 2014, 26, 2676-2682.
64. X. Lu, Y. Zeng, M. Yu, T. Zhai, C. Liang, S. Xie, M. S. Balogun and Y. Tong, Adv. Mater., 2014, 26, 3148-3155.
65. A. Ramadoss, B. Saravanakumar and S. J. Kim, Nano Energy, 2015, 15, 587-597.
66. Q. Huang, L. Liu, D. Wang, J. Liu, Z. Huang and Z. Zheng, J. Mater. Chem. A, 2016, 4, 6802-6808.
67. R. Worsley, L. Pimpolari, D. McManus, N. Ge, R. Ionescu, J. A. Wittkopf, A. Alieva, G. Basso, M. Macucci and G. Iannaccone, ACS nano, 2019, 13, 51 - 60.
68. D.G. Purdie, D. Popa, V.J. Wittwer, Z. Jiang, G. Bonacchini, F. Torrisi, S. Milana, E. Lidorikis, A. C. Ferrari, App. Phys. Lett., 2015, 25, 253101.

